Regular Article

PHYSICAL CHEMISTRY RESEARCH
Published by the
Iranian Chemical Society
www.physchemres.org
info@physchemres.org

Phys. Chem. Res., Vol. 13, No. 4, 797-816, December 2025
DOI: 10.22036/pcr.2025.538792.2715

Fe_3O_4/SBA-16-NH_2 Nanocomposites: Synthesis, Characterization and Applications as a Phenobarbital Drug Release Systems

M.H. Fekri*, M. Razavi Mehr and S. Soleymani

Department of Chemistry, Faculty of Basic Sciences, Ayatollah Boroujerdi University, Boroujerd, Iran

(Received 2 August 2025, Accepted 22 October 2025)

In this study, the Fe_3O_4/NH_2-SBA-16 mesostructure was synthesized as a nanocarrier for loading and release of the phenobarbital drug. To identify and characterize the properties of the SBA-16/NH_2 and Fe_3O_4/NH_2-SBA-16 nanostructures, several identification methods, such as X-ray diffraction analysis, Fourier transform infrared spectroscopy, nitrogen adsorption-desorption isotherm, elemental analysis, scanning electron microscopy and transmission electron microscopy images, were used. The effects of variables including pH, drug concentration, nanocomposite dose, temperature, and contact time on absorption efficiency were studied by the response surface methodology and design of experiments software. The encapsulation loading efficiency percent was surveyed by the Design of Experiment software, and the features of release were measured. The results show that the highest percentage of adsorption can be achieved by the optimization of the effective factors on the loading drug. Moreover, Fe_3O_4/NH_2-SBA-16 exhibited controlled drug release.

Keywords: Fe_3O_4/NH_2-SBA-16 nanocomposite, Drug delivery, Design of experiment, Drug release

INTRODUCTION

Drug delivery refers to new approaches in the field of safe drug transfer within the body at the required concentration. In traditional drug delivery systems, such as oral or injection, the drug is distributed throughout the body, and only a small percentage of the drug reaches the desired tissues [1,2]. Also, under the influence of stomach acid, enzymes and metabolic processes, peptides, and proteins are altered, degraded, or absorbed before entering the systemic circulation, and their bioavailability is greatly reduced. Nanotechnology has solved many aforementioned problems. Nanoparticles protect the drugs that are prone to degradation in the body from damage and increase the effect and efficiency of the drugs by prolonging the presence of the drug in the blood and the long release of the drug. The main goals in preparing pharmaceutical carriers are to reduce the particle size, increase the surface area, and release the drug at the desired location and with the appropriate speed and therapeutic dose [3-5]. Currently, most efforts emphasize the development of drug delivery techniques to the target tissue, for example, cancer tissues, and the gradual release of the drug from drug delivery carriers. To achieve this goal, the designed systems must be such that the body's defense system is not stimulated, and the carriers can exist in the body for a longer time and reach the target tissue [6,7].

Mesoporous nanoparticles are one of the newest and best nanoparticles that can be used in targeted drug delivery with the help of these nanocarriers. The drug is delivered to the target tissue at a specific time and place with appropriate efficiency and controlled release. Mesoporous protects the drug in the body and releases it in the target tissue [8,9]. An important and non-toxic group of these mesoporous compounds is the SBA family [10]. SBA-type mesoporous materials belong to the ceramic family and were first synthesized in 1998. These compounds have a pore size of 30-46 nm and have thick silica walls. SBA-16 is a three-dimensional cubic cage belonging to the space group Im3m among the mesoporous SBA compounds [11,12]. SBA-16

*Corresponding author. E-mail: m.h.fekri@abru.ac.ir

causes higher mass transfer due to its highly effective surface area and connected three-dimensional channels. Non-ionic surfactants are often used in the synthesis process of this porous mesoporous. These surfactants are usually oligomer surfactants based on alkyl poly (ethylene oxide) PEO with the general formula EOXPOYEOX, where the amount of x affects the wall thickness and the amount of y affects the size of the pores [13,14].

SBA-16 has parallel open mesochannels with narrow, tunable and uniform pore size distribution over a wide range from 6 to 12 nm, high pore volume, good thermal and chemical stability, controllable hydrophobicity or hydrophilicity, water insolubility, non-toxic [15], mechanical resistance, biocompatible and biodegradable, and a wall thickness of about 3 to 4 nm. Such properties make these materials suitable as carriers for drug delivery systems. However, these mesoparticles do not have diverse functional groups (mainly containing silane groups), which limits the possible applications of these materials for specific target molecules [16]. The Fe_3O_4 nanoparticles have electrical and magnetic properties. In addition, due to their biocompatible surface chemistry, high magnetic saturation value, narrow particle size distribution (less than 100 nm), far-field controllability, resonant response to field changes, and superparamagnetic properties, compared to other magnetic nanoparticles, they are very useful in the field of drug delivery [17]. Among the disadvantages of these compounds in drug delivery systems, we can mention the reduction of the external field to a certain extent and the high cost of preparing this carrier [18].

Numerous studies have shown that silica nanoparticles and magnetic nanoparticles have good biocompatibility and biodegradability. Furthermore, they are destroyed in the body over time. *In vitro* toxicity studies showed little toxicity at low concentrations for these compounds, but an increase at higher concentrations. It has been shown that toxicity is somewhat dependent on the particle size. In vivo studies have shown little toxicity for SBA-16 [19]. Mesoporous silica particles modified with iron oxide have shown low toxicity in the bodies of mice [20].

Nowadays, there are many physical and chemical methods for designing magnetic nanoparticles. Many efforts have been made to design, develop and improve magnetic nanoparticles to enable the production of highly pure nanomaterials on a mass scale, but controlling the shape and size of the nanoparticles is not easily possible. In general, three methods (physical, chemical, and biological) are used to synthesize magnetic nanoparticles. These methods are difficult to apply on a large scale due to the need for a high-energy, skilled researcher and complex optimized parameters. The main challenge in preparing magnetic nanoparticles for biomedical applications is to control the size, shape, distribution, magnetic properties, and surface chemistry of nanoparticles.

A disadvantage of nanoparticles is their separation from the liquid phase. The common method for separating nanoparticles from the liquid phase is using a centrifuge, and the efficiency of this method is low. One of the useful methods for separating nanoparticles from the solvent is to use magnetic particles in the nanocomposite structure and then easily separate them with a magnet. Magnetic separation is a process used in many industries to extract ferromagnetic and paramagnetic particles from mixtures. This process has advantages, the most important of which are the following: Magnetic separation is a clean process that does not require chemicals, so there are no environmental hazards. Magnetic separators are highly efficient in separating magnetic particles from non-magnetic materials and are ideal for applications where high purity levels are required. Magnetic separation can be used to recover a wide variety of magnetic materials, from ferromagnetic to paramagnetic particles. In this research, Fe_3O_4 magnetic nanoparticles were loaded on SBA-16/NH_2 by the *in situ* method [21].

By comparing the present study with other studies on the loading and release of phenobarbital drug, it was concluded that the nanocarrier prepared in this study has the ability to adsorb more drug and can also release the drug for a longer period of time. For example, in a study, solid lipid nanoparticles were used as carriers for the phenobarbital drug. The results of this study showed a loading rate of 98.2%, but the release studies showed that the drug was released quickly and the drug remained in the body for a shorter period of time [22]. In another study, magnetic nanoparticles were used as a carrier for the phenobarbital drug. The results of this research showed that this nanocarrier adsorbed only 61% of the drug, and 80% of the drug was released in 20 min [23]. Therefore, by comparing the nanocarrier prepared in this study with other studies, it can be

concluded that this carrier can be a more suitable carrier for phenobarbital due to its ability to achieve the highest drug loading and slow and stable release.

This study is unique in comparison to other studies in that it can be summarized as follows: In this study, the drug carrier used was material SBA-16, which has not been widely utilized in this field. Furthermore, this class of substances is pore-forming, and pore-forming substances are ideal for the regulated release of drugs. The surface was modified with the functional groups –NH2 in order to improve its efficiency. The nanoparticles, however, are challenging to separate because of their colloidal character. The produced nanoparticles can be separated from the solution using a magnet because of the magnetic Fe_3O_4 utilized in this study. The ideal conditions were then determined using the Design of Experiment program.

In this work, the characteristics of the Fe_3O_4/NH_2-SBA-16 nanocomposite prepared by the immersion method were evaluated using different analyses. After loading the phenobarbital (PHB) drug on the nanocomposite, the release of this drug was tested in vitro environment. For the optimization of the main effects of loading drugs onto the nanocomposite, the DOE software (CCD) model and the response surface method (RSM) were used. The parameters that were investigated included: pH, the amount of adsorbent, drug concentration, temperature, and contact time. Three models were used to determine the synthetic model of drug loading on the nanocomposite: Freundlich, Langmuir, and Temkin isotherms. Thermodynamic, drug loading, and release kinetics studies were conducted to determine the thermodynamic and kinetic parameters.

The highlight of the present work is that by optimizing the silica surface, the active sites for loading the drug will increase and the percentage of adsorption will increase up to about 99%. One of its disadvantages is related to the separation of SBA-16-NH_2 from the liquid phase after the adsorption of the phenobarbital drug from water. The conventional method for separation from the liquid phase is filtration. However, filtration causes the filters to clog and some SBA-16-NH_2 to be lost. Therefore, researchers are looking to find new ways to separate nanoparticles from the liquid phase. One of these methods is to create a magnetic property in nanoparticles and then easily separate them with a magnetic field [24,25]. In this work, by magnetizing SBA-16-NH_2 with Fe_3O_4, we easily separated it from the aqueous environment. Another important work is the determination of the affective factors on drug adsorption using experimental design as a time method that minimizes the amount of error in the result of adsorption percent. In this way, knowing the influence coefficient of each of the effective parameters in adsorption, the desired adsorption can be reached. In this work, an experimental design has been used for the industrial production of nanocarriers, and the conditions can be changed selectively. Also, due to the high specific surface of the nanocarrier, a small amount of the nanocarrier can be used to carry a large amount of medicine, which is economically viable.

EXPERIMENTAL

Chemicals

Pluronic f127 copolymer, 3-aminopropyltriethoxysilane (APTEOS), and tetraethylorthosilicate (TEOS) were obtained from Sigma-Aldrich Company. To prepare Fe_3O_4 magnetic nanoparticles, $FeCl_3.6H_2O$ and $FeCl_2.4H_2O$ were produced by Merck Co. Phenobarbital drug (PHB) with the formula $C_{12}H_{12}N_2O_3$ (Sigma Aldrich). NaH_2PO_4 and NaO_2HPO_4 were used to prepare buffer solutions as a simulated body environment. A dialysis bag with an average flat width of 23 mm was used to release the drug (Sigma Aldrich Company).

Apparatus

An AXS-D8Advance device (Netherlands) was used for the X-ray diffraction measurements X-ray diffraction. Morphology studies were performed using a scanning microscope (SEM) model FESEM, Czech Republic and a transmission microscope (TEM) with models HITACHI, S-3400N, Japan, and EM208S 100KV, respectively. The functional groups of the SBA-16, Fe_3O_4, SBA-16/NH_2, and Fe_3O_4/NH_2-SBA-16 structures were identified using Fourier transform spectroscopy (FTIR) with models Magana550, Perkin Elmer-Spectrum65, USA. Spectrophotometric measurements and BET analysis were performed using a UV/Vis spectrophotometer (Dynamica-HALO-DB-20, Germany) and a nitrogen (N_2) adsorption-desorption isotherm at 77 K temperature to check the surface area, size, and volume of pores, respectively (NanoSORD92, Japan).

Thermal analysis (TG) was performed under a nitrogen environment at 1000 °C and a speed of 5 revolutions per minute by the TA company model Q600 made in the USA. Also, in this research, a centrifuge (Gama Teb-X-400 rpm, Iran), pH meter (ST2100, Switzerland), magnetic stirrer (Labinco-L81ST, Netherlands), oven (Memmert, Germany), oven (Shimazo, Iran), and ultrasonic (Elmasonic-S, Germany) were used.

Synthesis of Fe_3O_4

Fe_3O_4 magnetic nanoparticles were prepared using the Stopper method [26,27]. First, $FeCl_2.4H_2O$ and $FeCl_3.6H_2O$ were dissolved in 10 ml of distilled water (0.994 and 2.702 g, respectively). Then, the sample was stirred in a three-hole beaker under a nitrogen atmosphere. Then, 20 ml of ammonia was added to the flask under stirring (pH~9). The obtained precipitate (black color) was separated from the solvent by a magnet and washed with 96% ethanol. Finally, the Fe_3O_4 nanoparticles were dried in an oven at 65 °C for 18 h. The summary of the reaction of the Fe_3O_4 preparation is shown in the following equation.

$$2Fe(III) + Fe(II) + 8OH^- \rightarrow Fe(OH)_2 + 2Fe(OH)_3 \rightarrow Fe_3O_4 + 3H_2O \quad (1)$$

Synthesis of SBA-16/NH_2

In this work, to increase the efficiency of SBA-16, it was functionalized by the $–NH_2$ group [28]. For the preparation of SBA-16/NH_2, 3 g of F127 copolymer was dissolved in 144 ml of distilled water and 9 ml of HCl. After stirring for about half an hour, 9 ml of 1-butanol was added to the mixture. After one hour, specific amounts of ingredients (TEOS and APEOS) were added to the mixture. The mixture was stirred for 24 h at 35 °C. Then it was placed in an oven at 100 °C for 24 h. Finally, the template was removed using ethanol extraction.

Synthesis of Fe_3O_4/NH_2-SBA-16

In this work, 60 mg of Fe_3O_4 was dispersed in 20 ml of ethanol, and then 0.2 g of SBA-16/NH_2 was added to it and mixed for 8 h at ambient temperature. Then, the prepared nanocomposite was separated from the solvent by a magnet and dried at room temperature.

Drug Loading on Fe_3O_4/NH_2-SBA-16 Nanocarrier

To load the phenobarbital drug, solutions with concentrations of 10, 20, 30, 40, and 50 ppm were prepared from the PHB drug. Then, 50 ml of each of these solutions were mixed with specific amounts of Fe_3O_4/NH_2-SBA-16 nanocarrier (0.01, 0.02, 0.03, 0.04, and 0.05 g) and 15 min were placed in the ultrasonic and then stirred by a magnetic stirrer for 3 h. Then the samples were and it was separated by a magnet. The amount of drug loading was obtained from Eq. (2):

$$EE\% = \frac{(C_0 - C_e)}{C_0} \times 100 \quad (2)$$

where C_0 (initial concentration) and C_e (residual concentration) were obtained from UV-Vis spectrometry.

Potential Zero Charge (PZC) of Phenobarbital

A solution with a concentration of 1000 ppm of the drug was prepared, and more dilute solutions were prepared using this stock solution., Then the absorbance of these solutions was read at the maximum wavelength of the phenobarbital drug (λ_{max} = 276 nm).

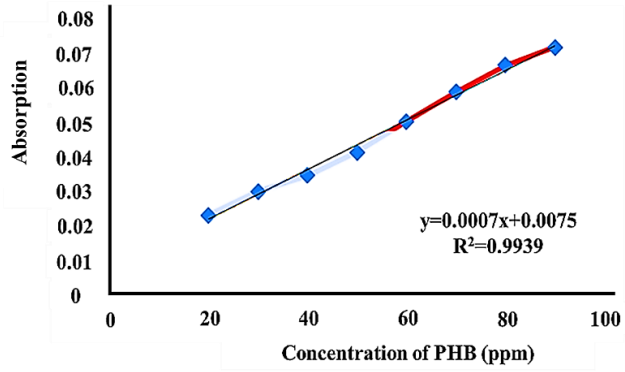

Fig. 1. Calibration curve of PHB drug.

The pH_{PZC} was determined by dissolving the PHB drug in 15 ml of distilled water, and the pH of the solution was read in the range of 2 to 12 as the initial pH. At zero-point pH, positive and negative surface charges are equal [29].

Then, the final pH of the solution was read again after stirring for 2 h. According to Fig. 2, pH_{PZC} was obtained equal to 6.5.

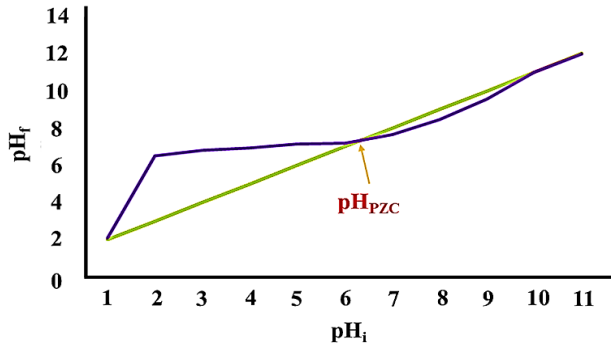

Fig. 2. The pH_{PZC} of PHB Drug.

Experimental Design

One of the important goals of the drug delivery process is to determine the optimal value of drug adsorption on the drug carrier. It is essential to study the influencing factors on the amount of drug adsorption on the nanocarrier. One of the useful methods in parameter optimization is the use of main effects and pairwise interactions of factors affecting the response [30]. Therefore, experiments were performed for five parameters, initial nanocomposite dose, drug concentration, contact time, and temperature at five levels. The proposed tests of the software are reported in Table 1, and the results were fitted using Eq. (2):

$$Y = \beta_0 + \sum_{i=1}^{5} \beta_i X_i + \sum \beta_{ij} X_i X_j \quad (3)$$

where Y is a symbol of the response, X_i and X_j are the main effects symbols, and β is the fitting coefficient. Our goal is to find these coefficients. The software has predicted 50 tests for the load of the drug onto the Fe_3O_4/NH_2-SBA-16 nanocomposite (Table 2).

Drug Release

Drug release was performed using a dialysis bag in three neutral, acidic, and alkaline environments as an external solution or simulated body environment. The neutral medium was distilled water with pH = 6.8, and the acidic and alkaline mediums were buffer solutions with pH 4.8 and 7.4, respectively. A solution of 500 ml was prepared from each of the external environments. Then, the dialysis bag containing the drug solution and nanocarrier was transferred inside them. This set was placed on a magnetic stirrer. Drug release experiments were tested at 1, 2, 3, 4, 12, 24, 48, and 72 h.

RESULTS AND DISCUSSIONS

FT-IR Spectrum

For studying the functional groups in the SBA-16/NH_2 and Fe_3O_4/NH_2-SBA-16 nanoparticles, the FT-IR spectrum was used (Fig. 3). The sign of the presence of the stretching and bending vibrations of the Si-OH functional group has been identified at 3441.12 cm^{-1} and 1630.95 cm^{-1}, respectively [31]. The bonds observed at 1086.21 cm^{-1} and (797.37 and 949.10 cm^{-1}) show the asymmetric and symmetric stretching vibrations of Si-O-Si. Also, the bands observed in 471.94 cm^{-1} were assigned to tetrahedral SiO_4. The bands assigned to the N-H stretching vibrations around 2930.52 cm^{-1} indicate the presence of the -NH_2 group [27,32].

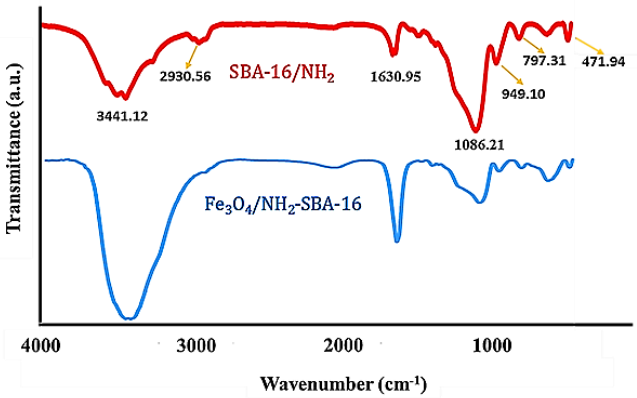

Fig. 3. FTIR peaks of SBA-16/NH_2 and Fe_3O_4/NH_2-SBA-16 in the region of 4000-400 cm^{-1}.

Table 1. Effective Factors of Drug Loading by the Fe_3O_4/NH_2-SBA-16 Nanocarrier by CCD Design

Parameter	Component	Unit	Applied level				
			(-2)	(-1)	(0)	(+1)	(+2)
A	pH	-	2	4	6	8	10
B	NCD	g	0.01	0.02	0.03	0.04	0.05
C	ICT	ppm	10	20	30	40	50
D	Temp.	°C	30	40	50	60	70
E	CT	min	10	20	30	40	50

Table 2. The Proposed Software Tests and Experimental Results at Low, center and High Levels

Row	pH	NCD (g)	ICD (ppm)	Temp. (°C)	CT (min)	EE%
1	+2	0	0	0	0	47
2	-1	-1	+1	+1	-1	78.25
3	0	0	-2	0	0	79.50
4	+1	+1	-1	-1	+1	66.75
5	+1	-1	-1	-1	-1	60.50
6	0	+2	0	+2	0	87.50
7	+1	+1	+1	+1	_-1	60.00
8	0	0	0	0	0	79.25
9	+1	+1	-1	-1	-1	67.50
10	+1	-1	+1	+1	-1	57.00
11	-1	-1	+1	-1	-1	89.75
12	0	0	+1	0	0	72.50
13	+1	-1	-1	+1	+1	56.10
14	-2	0	0	0	0	98.50
15	0	0	0	0	0	78.25
16	-1	+1	-1	+1	+1	99.00
17	0	0	0	0	0	80.25
18	-1	+1	-1	-1	+1	99.50
19	0	0	0	0	0	80.50
20	-1	-1	-1	+1	-1	82.00
21	-1	+1	-1	+1	-1	93.00
22	-1	-1	-1	-1	-1	89.50
23	-1	-1	+1	-1	+1	89.20
24	0	0	0	-2	0	78.50
25	+1	-1	+1	-1	+1	65.00
26	0	0	0	0	-2	69.50
27	+1	-1	+1	+1	+1	61.00
28	-1	+1	-1	-1	-1	95.00
29	+1	+1	-1	+1	-1	62.50
30	0	0	0	0	0	79.50
31	+1	-1	+1	-1	-1	65.50
32	-1	-1	+1	+1	+1	82.00
33	0	0	0	0	0	78.00
34	+1	+1	-1	+1	+1	66.50
35	+1	-1	-1	+1	-1	56.50
36	-1	-1	-1	-1	+1	87.00
37	-1	+1	+1	+1	+1	86.00
38	-1	+1	+1	+1	-1	78.00
39	-1	-1	-1	+1	+1	57.50
40	-1	-1	+1	+1	+1	85.20
41	0	0	0	0	0	79.50
42	0	0	0	0	+2	77.00
43	0	0	0	+2	0	67.50
44	0	0	0	0	0	78.50
45	+1	+1	+1	-1	+1	90.50
46	+1	+1	+1	+1	+1	61.50
47	0	-1	0	0	0	80.75
48	+1	+1	+1	-1	+1	65.00
49	-1	+1	+1	-1	-1	86.00
50	+1	+1	+1	+1	-1	55.00

XRD Diffraction Patterns

Figure 4a provides the XRD analysis of mesoporous SBA-16/NH_2, which presents a sign of the preparation of porous materials in the range of 2θ = 20-30° [33]. In Fig. 4b, the XRD pattern of the sample Fe_3O_4/NH_2-SBA-16 is shown. The XRD patterns of the synthesized Fe_3O_4/NH_2-SBA-16 nanoparticles show six peaks at 2θ = 31, 35, 44, 54, and 63° with Bragg peaks at (220), (311), (400), (422), (511), and (440), respectively, related to the Fe_3O_4 nanoparticles. The XRD pattern of the Fe_3O_4/NH_2-SBA-16 nanoparticles shows another peak around 2θ = 20-30°, which can be referred to as the existence of the non-crystalline part of the composite [34].

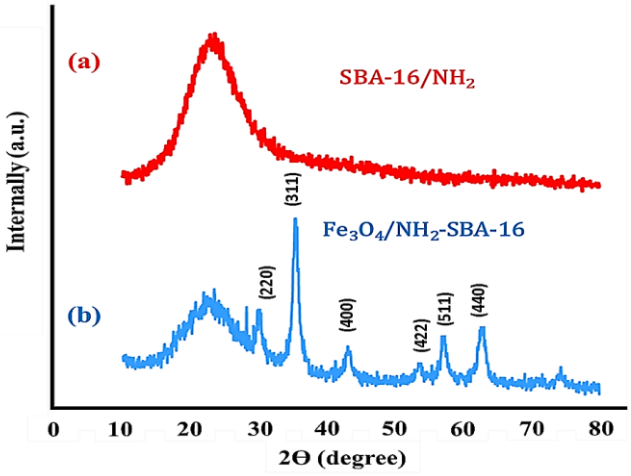

Fig. 4. XRD patterns of (a) SBA-16/NH_2 and (b) Fe_3O_4/NH_2-SBA-16 nanoparticles.

SEM, TEM and EDAX Analyses

The electron microscopy images (SEM and TEM) and the EDAX spectrum of the synthesized Fe_3O_4/NH_2-SBA-16 sample are shown in Fig. 5. We can conclude with the help of the SEM images (Figs. 5a, b) that the synthesized Fe_3O_4/NH_2-SBA-16 nanocomposite has a spherical and homogeneous morphology. Also, as shown in the figure, the size of the nanoparticle pores is between 2-50 nm, which confirms the mesoporous nature of the nanocomposite. [35]. Scanning electron microscope images (TEM) of the Fe_3O_4/NH_2-SBA-16 nanocomposite (Fig. 5c) show that the Fe_3O_4 particles were successfully placed on the SBA-16/NH_2 mesostructure (black spots). As it is clear from the TEM images, the morphology of SBA-16/NH_2 is maintained after the placement of Fe_3O_4 and no significant change is observed in it [33,36]. In addition, the EDAX spectrum shows (Fig. 5d) elements in the Fe_3O_4/NH_2-SBA-16 nanocomposite structure that include C, O, N, Si, and Fe atoms.

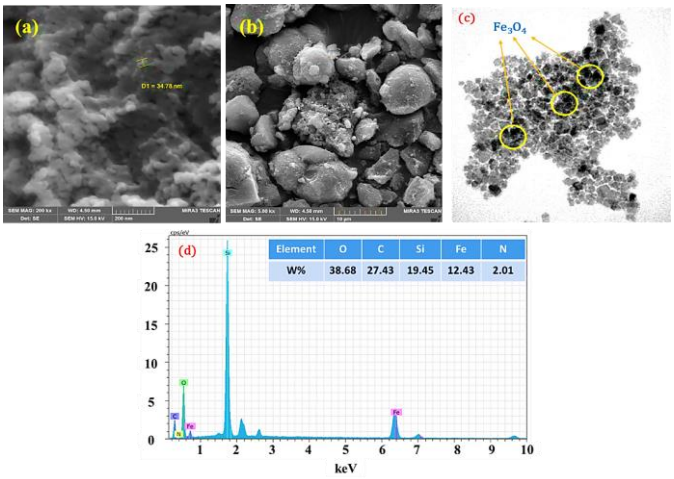

Fig. 5. SEM micrograph (a, b), TEM micrograph (c), and EDX graph (d) of Fe_3O_4/NH_2-SBA-16.

TG Analysis for SBA-16/NH_2 Sample

Thermal gravimetric analysis (TGA) was performed to study the thermal stability of the samples (Fig. 6). The mass loss at ~20-200 °C corresponds to the release of the absorbed moisture. At higher temperatures, the decomposition of the amine group began and was completed at 800 °C. For samples modified with amine groups, only one main peak was observed at 400 °C.

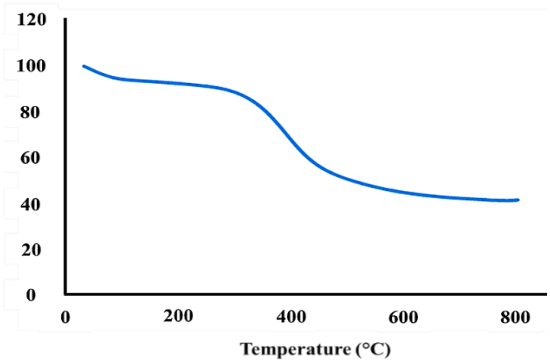

Fig. 6. SBA-16/NH_2 thermal gravimetric diagram.

Nitrogen Adsorption/Desorption Analysis (BET Analysis)

Figure 7 illustrates the adsorption and desorption isotherm and pore size distribution of the Fe_3O_4/NH_2-SBA-16 nanocarrier. As shown in Fig. 7a, which can be demonstrated as the type IV(a) isotherm corresponds to the IUPAC nomenclature of the isotherms, and the absorption/desorption process formed a hysteresis loop [37]. Also, by using the adsorption/desorption isotherm, we will be able to identify the geometry of the holes. According to the diagram (Fig. 7a), the holes have a cylindrical geometry [38,39]. The BJH curve in the range of 1-100 nm is shown in Fig. 7b. Using this curve, the distribution of the holes can be measured. As can be seen, the maximum distribution of holes is in the range of ~1-50 nm. Also, the BET results of the Fe_3O_4/NH_2-SBA-16 nanocomposite indicate that the specific surface area of the Fe_3O_4/NH_2-SBA-16 nanocomposite is 19.158 m^2/g. Also, the average particle diameter and pore volume are 17.894 nm and 0.086 $cm^3\ g^{-1}$, respectively.

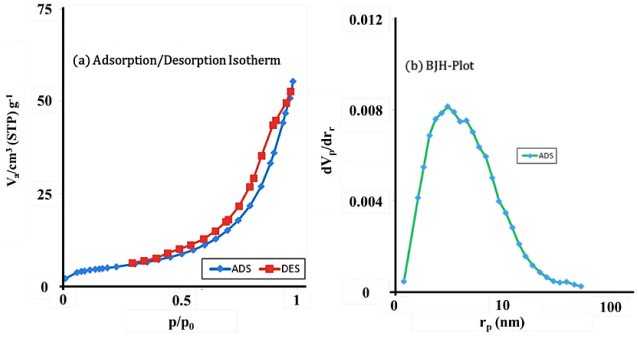

Fig. 7. (a) Adsorption/desorption isotherm and (b) BJH-plot for checking the pore size distribution of the Fe_3O_4/NH_2-SBA-16 nanocomposite.

Experimental Design

The normal probability curve shows how the residual values follow a normal distribution. Even though the data follow a normal distribution, some average distribution is expected. Therefore, the results show that the data have a normal distribution and are consistent with the model proposed by the software (Fig. 8a). The graph of the actual values versus the predicted values is shown in Fig. 8b which states a good agreement between the actual and predicted values (Fig. 8b). The curve of the standard residual values versus the responses can be seen in Fig. 8c. According to the figure, all the results are within the confidence range of -4 to +4, which indicates a good fit between the model and the answers obtained. According to Fig. 8d, all the results are within the confidence range of -3 to +3, which shows a random distribution. It is concluded that the model can describe the responses.

After the tests, the results are given to the software to provide the best model for evaluating and describing the data. Among the 4 linear, interaction, quadratic, and cubic models, the software's proposed model was the quadratic model, which was the most consistent with the answers. As can be seen in Table 3, the quadratic model has a probability value of less than 0.05 and the highest regression coefficient (0.9945) compared to the other 3 models, that show the most suitable model.

ANOVA analysis was performed by operating a quadratic accurate model (Table 4). It shows the main effective factors on the encapsulation of phenobarbital drug on the Fe_3O_4/NH_2-SBA-16 nanocomposite separately and their interactions based on the proposed software model.

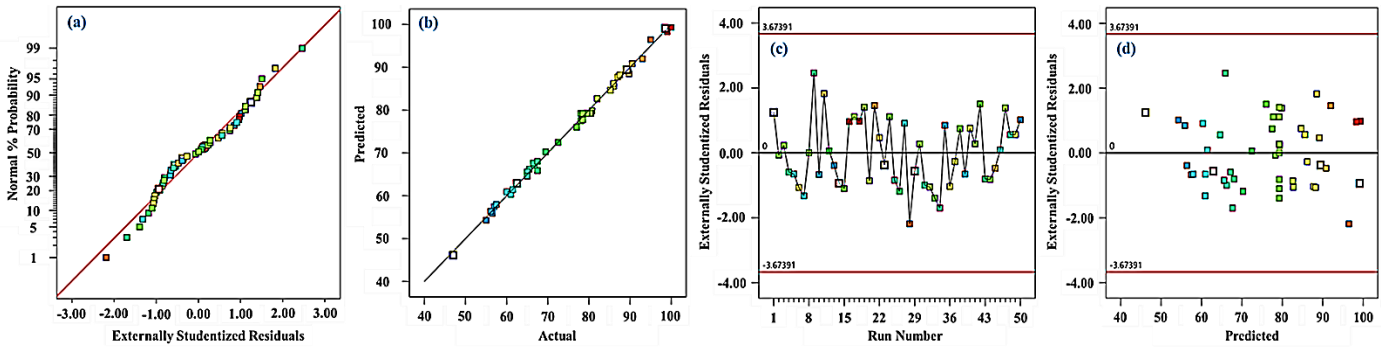

Fig. 8. Graphical plots of the experimental design.

Table 3. The Appropriate Model Based on the Statistical Analysis Suggested by the DOE Software

Source	Sequential p-value	Lack of fit p-value	Adjusted R^2	Predicted R^2	
Linear	< 0.0001	0.0001	0.9011	0.8843	
2FI	0.0009	0.0006	0.9420	0.9404	
Quadratic	< 0.0001	0.4462	0.9945	0.9898	Suggested
Cubic	0.1999	0.6537	0.9958	0.9838	Aliased

Table 4. ANOVA Analysis Based on the Suggestion Model

Source	Sum of squares	D. f.	Mean square	F. v.	P. v.	
Model	8338.22	20	416.91	446.51	< 0.0001	Significant
A-pH	7010.58	1	7010.58	7508.29	< 0.0001	
B-comp. dose	175.35	1	175.35	187.80	< 0.0001	
C-cons. drug	118.51	1	118.51	126.92	< 0.0001	
D-temp.	235.95	1	235.95	252.70	< 0.0001	
E-cont. time	81.94	1	81.94	87.76	< 0.0001	
AB	11.22	1	11.22	12.02	0.0017	
AC	69.47	1	69.47	74.40	< 0.0001	
AD	4.39	1	4.39	4.70	0.0385	
AE	4.92	1	4.92	5.27	0.0291	
BC	208.34	1	208.34	223.13	< 0.0001	
BD	8.66	1	8.66	9.28	0.0049	
BE	36.66	1	36.66	39.26	< 0.0001	
CD	26.74	1	26.74	28.63	< 0.0001	
CE	11.46	1	11.46	12.27	0.0015	
DE	24.24	1	24.24	25.96	< 0.0001	
A^2	86.96	1	86.96	93.13	< 0.0001	
B^2	45.72	1	45.72	48.97	< 0.0001	
C^2	22.36	1	22.36	23.95	< 0.0001	
D^2	80.49	1	80.49	86.20	< 0.0001	
E^2	74.27	1	74.27	79.54	< 0.0001	
Residual	27.08	29	0.9337			
LOF	21.27	22	0.9670	1.17	0.4462	Not significant
PE	5.80	7	0.8292			
CT	8365.30	49				

D. f.: Degree of freedom **F. v.**: F-value **P. v.**: P-value
LOF: Lack of fit **PE**: Pure error **CT**: Core total.

The p-value and lack of fit are among the statistical parameters that are used to measure the validity and accuracy of the investigated model. When the p-value is greater than 0.05 for the factors, the factor is of little importance and does not play a role in the final model. As can be seen in Table 4, all the parameters have p-values less than 0.05, which indicates the correct relationship between the factors and parameters. The lack of fit value is predicted by Adjusted R^2 and Predicted R^2 coefficients, and their values change between 0 and 1. Their proximity to 1 indicates that the model is more appropriate. In this experiment design, the values of Adjusted R^2 and Predicted R^2 coefficients were obtained at 0.9945, 0.9974 and 0.9898, respectively [10].

In this experiment, the sum of R-squared ($R^2 = 0.9968$). The predicted R agrees with the actual R. The difference is less than 0.2. The ratio of 8471/84 obtained for Adeq Precision shows the appropriateness of the proposed software model. The coded equation related to all of the considered parameters and their interactions is as follows:

$$\boldsymbol{EE}\% = +79.24 -13.24A +2.09B -1.72C -2.43D +1.43E -0.59AB +1.47AC +0.37AD -0.39AE -2.55BC +0.52BD +1.07BE -0.91CD +60CE +0.87DE -1.65A^2 +1.20B^2 -0.84C^2 -1.59D^2 - 1.52E^2 \quad (3)$$

Figure 9 shows the effect of 5 parameters: the pH, composite dosage, drug concentration, effect of temperature, and contact time factors on the encapsulation of the drug.

Experiments related to phenobarbital drug loading were performed at pH values of 2, 4, 6, 8, and 10. The maximum amount of encapsulated Fe_3O_4/NH_2-SBA-16 nanocomposite was obtained at pH = 2.6 (Fig. 9a). The results showed that the pH value has an inverse relationship with the drug load. The interaction between the drug and the nanocomposite at low pH is greater due to electrostatic forces, so the loading increases with the decrease in pH. The adsorbent used in this work has a pH of zero charge (pH_{pzc}) of 6.5 (Fig. 2), which means that the adsorbent has a positive charge at pH < 6.5, neutral at pH = 6.5, and negative charges at pH > 6.5. At low pH (lower than the pH of zero charges = 6.5), H^+ ions are placed on the nanocomposite sites, and the nanocomposite surface becomes more positive. Considering that the surface of the phenobarbital drug is negatively charged due to the amine groups, at low pH, due to the electrostatic attraction between the adsorbent and the drug, the percentage of drug loading increases. However, at high pH (higher than pH_{pzc}), OH^- ions increase on the surface of the nanocarrier, and the repulsion between the surface and the drug reduces the amount of drug loading [40].

The effect of the dosage of the Fe_3O_4/NH_2-SBA-16 nanocomposite on the amount of EE% was investigated (Fig. 9b), which had a positive effect (p-value < 0.05). It was seen that the amount of the nanocomposite has a direct relationship with the drug loading. Because when the amount of the nanocomposite increases, there are more places on the surface of the nanocomposite available for the drug to interact. The maximum amount of the nanocomposite for drug loading is 0.05 g.

The initial concentration of the PHB drug and the temperature parameters presented a negative effect on the EE% (Figs. 9c & 9d). Therefore, increasing the concentration of PHB and temperature decreased the loading. It seems that due to the saturation of the active sites on the nanocomposite Fe_3O_4/NH_2-SBA-16, the drug loading decreases with increasing drug concentration. The effect of temperature on the EE% was studied at 30, 40, 50, 60, and 70 °C. A decrease in loading can be attributed to changes in the Gibbs free energy. In the adsorption process, the enthalpy changes are negative (exothermic) and the entropy changes are positive. According to the equation of $\Delta G = \Delta H - T\,\Delta S$, with the decrease in temperature. In this way, the absorption process becomes spontaneous due to the negative free energy of Gibbs.

The contact time required to achieve stable absorption is directly proportional to the drug loading capacity (Fig. 9e). In the initial stages, the speed of drug interaction with the nanocomposite is high, due to the availability of more vacancies

Figure 10 shows the diagram of the reciprocal effects of the parameters affecting drug loading. Optimum values obtained by graphic analysis and using Design Expert software can be extracted as surface curve and contour curve (Fig. 10) diagrams. These diagrams show the simultaneous effect of the two variables on the percentage of drug loading by the drug carrier. We examine the interaction of some variables as an example. Figures 10a, 10b and 10c show the interaction between (A/C), (B/C), and (B/D) with the values of the RC parameters +1.47, -2.55, and +0.52, respectively.

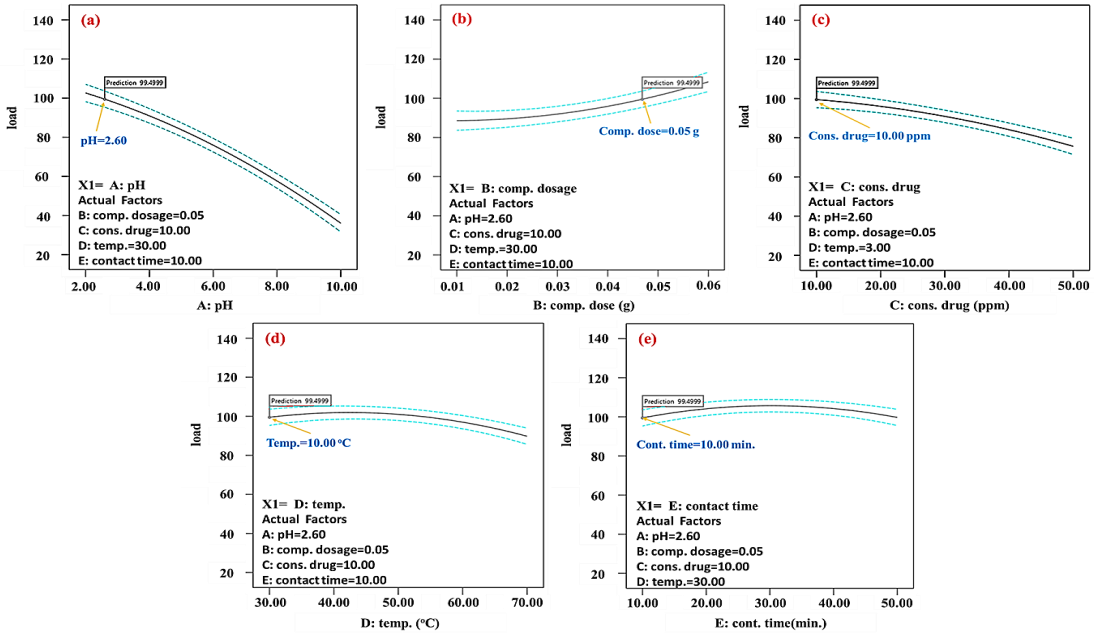

Fig. 9. The effect of important parameters on EE percent of the Phenobarbital drug by the Fe_3O_4/NH_2-SBA-16 nanocomposite.

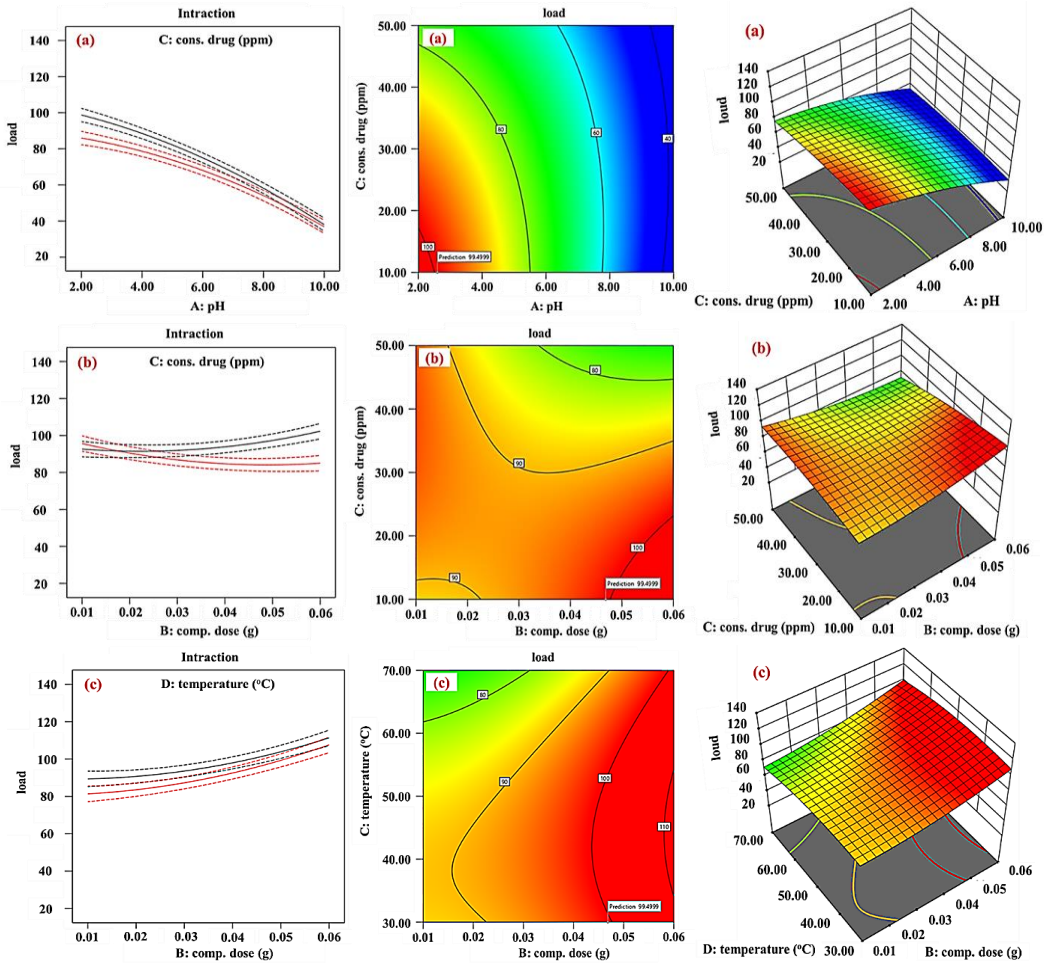

Fig. 10. Interaction, contour, and response surface plots %.

The graphs show that there is a non-parallel interaction between both components (Fig. 10a). Non-parallel lines indicate an interaction between the two components [41]. As the contour graph moves toward the red color, each factor provides a better level of response. For example, in the contour graph (Fig. 12a), the percentage of drug loading is shown as a function of pH and the nanocomposite. As can be seen in the figure, with decreasing pH and increasing nanocomposite amount, the percentage of drug loading increases, which indicates that these two factors have non-parallel effects. In Fig. 12b, it is observed that with decreasing pH and decreasing initial drug concentration, drug loading increases, which indicates the parallel effects of these two variables. In these diagrams, the red areas indicate the highest amount of drug loading.

Optimization of Encapsulation Efficiency

To achieve the maximum drug adsorption on the mesoporous Fe_3O_4/NH_2-SBA-16, the effective parameters were optimized using the experimental design software (Table 5). The software suggested an optimal value for each parameter. By performing the loading test, EE% values were calculated and compared with the value obtained by the suggested equation by the software. The Results showed a small difference between the experimental and predicted values (ΔEE% = 0.9) with a desirability of 0.95.

Isotherm Parameters

In this research, three important isotherms were considered under optimal conditions (pH = 2.60, comp. dose of nanocomposite 0.05 g, drug concentration 10.00 ppm, contact time 10 min, and temperature 30 °C) [42,43]. The Langmuir isotherm is one of the most valid laws of physical adsorption that is true in many cases. It is used for the adsorption of one layer on surfaces with a limited number of adsorption sites. Langmuir's linear equation is as follows.

$$\frac{1}{q_e} = \left(\frac{1}{bq_{max}}\right)\frac{1}{C_e} + \frac{1}{q_{max}} \qquad (4)$$

where q_e is the concentration of the adsorbed drug (mg/g) at any time, q_{max} is the maximum adsorption quantity by the adsorbent (mg g^{-1}).

The equilibrium constant k_l depends on the tendency of the adsorbent-adsorbate, and C_e is the equilibrium concentration of the drug (mg g^{-1}).

The Freundlich adsorption isotherm is valid for adsorption on heterogeneous surfaces. The Freundlich linear equation is as follows:

$$\log q_e = \log k_f + \frac{1}{nf} log C_e \qquad (5)$$

k_f and n are the Freundlich model constants that indicate the adsorption quantity and intensity, respectively.

The third isotherm studied in this work is the Temkin isotherm, which is expressed by the following equation:

$$q_e = BlnA + BlnC_e \qquad (6)$$

where B is a constant value related to the heat of adsorption and is defined by B = RT/b, b is the Temkin constant (J mol^{-1}), T is the absolute temperature (K), and R is the gas constant (8.314 J mol^{-1} K^{-1}). In addition, A is the Temkin isotherm constant (l g^{-1}).

The calculated constants for all three isotherms and their correlation coefficients (R^2) were calculated at the optimum temperature (Table 6 and Fig. 12). The results show that the Langmuir model (R^2 = 0.9989) is more suitable than the other model, which shows that the adsorption of PHB on Fe_3O_4/NH_2-SBA-16 is a physical method [44-46]. In other words, it can be concluded that the adsorption is a monolayer by suggesting the following mechanism (Fig. 11) [47].

Table 5. The Values of the Optimal Parameters and EE% (Predicted and Experimental)

ΔEE%	Desirability	EE% (Experimental value)	EE% (Predicted value)	pH	NCD	ICT	Temp.	CT
0.90	0.95	98.96	99.50	2.60	0.05	10.00	30.00	10.00

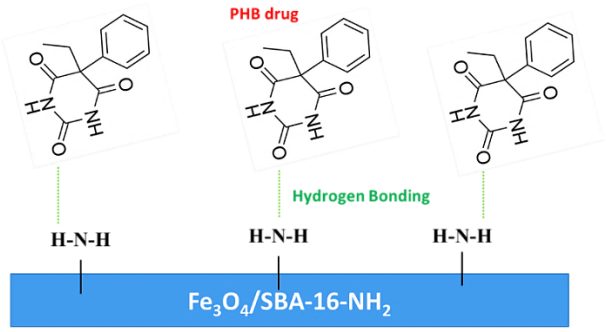

Fig. 11. The proposed mechanism for the adsorption of phenobarbital drug onto Fe_3O_4/NH_2-SBA-16.

One of the important factors in the quality of adsorption in the Langmuir isotherm is the separation factor (R_L), which is obtained from Eq. (7):

$$R_L = \frac{1}{K_L C_0} \quad (7)$$

If the value of the separation factor is between 0 and 1, it indicates the desirability of adsorption, and if it is more than 1, the adsorption is not desirable. In this work, the value of the separation factor (R_L) is 0.15. The result was that the adsorption of the PHB drug on the Fe_3O_4/NH_2-SBA-16 carrier used was desirable.

Table 6. Isotherm Parameters for PHB Loading onto Fe_3O_4/NH_2-SBA-16

50 ppm	40 ppm	30 ppm	20 ppm	10 ppm	Parameters	Model
15.0	9.1	3.5	1.4	0.5	C_e (ppm)	
26.92	23.76	20.38	14.30	7.30	q_e	Lungmuir
0.037	0.042	0.049	0.069	0.136	$1/q_e$	
0.066	0.109	0.285	0.714	2.000	$1/C_e$	
	R^2 = 0.9989	K_L= 0.68 l mg^{-1}		q_{max} = 28.9		
15.0	9.1	3.5	1.4	0.5	C_e (ppm)	
26.92	23.76	20.38	14.30	7.30	q_e	Freundlich
1.430	0.042	1.309	1.150	0.863	$\log q_e$	
1.17	1.37	0.54	0.14	-0.30	$\log C_e$	
	R^2 = 0.9297	K_f = 10.98 (mg/g) (l mg^{-1})n		n = 2.71		
15.0	9.1	3.5	1.4	0.5	C_e (ppm)	
26.92	23.76	20.38	14.30	7.30	q_e	Temkin
3.292	3.168	3.014	2.660	1.987	$\ln q_e$	
2.70	2.20	1.25	0.33	-0.69	$\ln C_e$	
	R^2 = 0.9271	K_T = 1.87		B = 0.367		

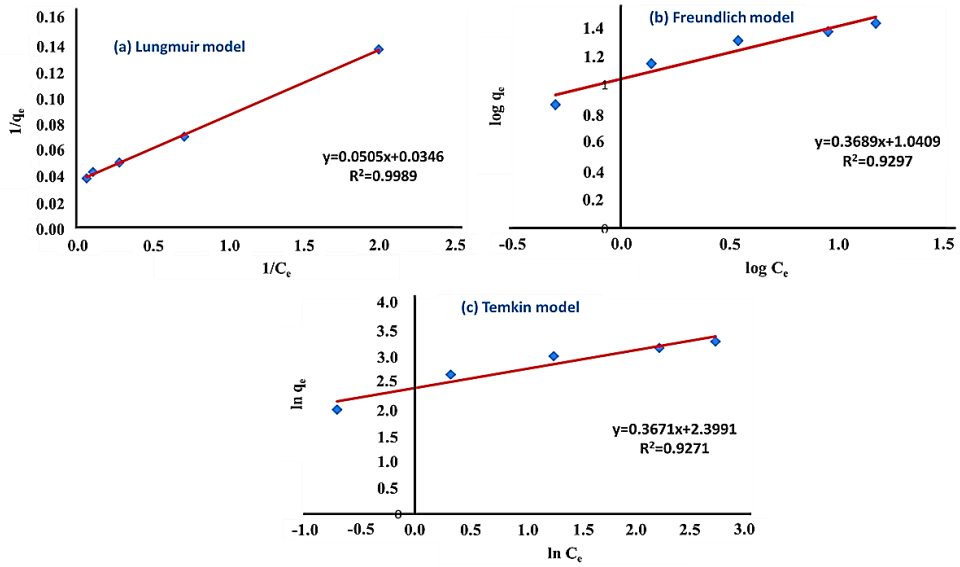

Fig. 12. Graphs of phenobarbital drug absorption on the adsorbent.

Thermodynamic Functions for Loading of PHB

The values of q_e and C_e were measured to calculate the thermodynamic functions of the PHB drug absorption onto the Fe_3O_4/NH_2-SBA-16 mesoporous at five temperatures of 303, 313, 323, 333, and 343 K under optimal conditions (Table 7). Using the following equations, the values of the thermodynamic functions were calculated [48,49]:

$$\ln K_c = -\frac{\Delta H^\circ}{RT} + \frac{\Delta S^\circ}{R} \quad (8)$$

$$\Delta G^\circ = -RT\ln K_c \quad (9)$$

$$\Delta G^\circ = \Delta H^\circ - T\Delta S^\circ \quad (10)$$

The values of ΔH° and ΔG° show that the adsorption of the phenobarbital drug on the Fe_3O_4/NH_2-SBA-16 adsorbent is physical and the process is spontaneous. The plot of $\ln K_c$ *vs.* 1/T is shown in Fig. 13.

ΔH°, ΔS°, and ΔG° values were determined as negative for the five studied temperatures, 303, 313, 323, 333, and 343 K. The negative values of ΔG° indicate that the adsorption process on the nanocarrier is spontaneous. It can be seen that ΔG° values turn out to be extra positive with the increase in temperature, so the increase in temperature isn't always desired in the adsorption process. The negative values of ΔH° indicated that the adsorption of PHB onto the nanocarrier is an exothermic process. The ΔS° values play a vital function in reflecting whether the order of the adsorbate throughout the adsorption process will become less random, $\Delta S^\circ < 0$, or more random, $\Delta S^\circ > 0$. Furthermore, the negative value of ΔS° includes reducing the degree of freedom of the PHB drug inside the solution. According to the value ΔH°, the adsorption between the drug and the nanocarrier could be categorized as physical adsorption. Physical adsorption is based on weak reactions between the adsorbate and the surface sites of the adsorbent.

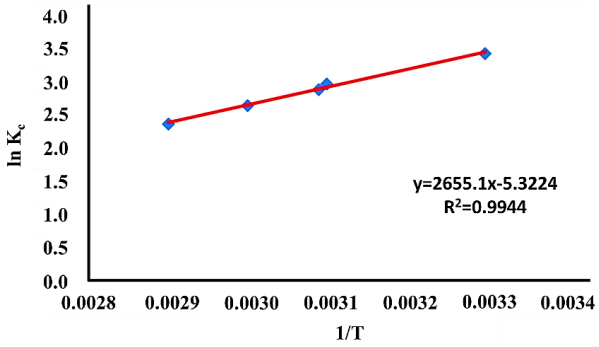

Fig. 13. Linear plot of $\ln K_c$ vs 1/T for the adsorption of the PHB drug onto Fe_3O_4/NH_2-SBA-16.

Kinetics Studies for Loading of PHB

Four kinetic models using the following equations were investigated to choose the best kinetic model (Fig. 14 and Table 8) [50].

zero order (ZO) model: $$q_t = k_0 t + q_0 \quad (11)$$

pseudo first order (PFO) model: $$\ln(q_e - q_t) = -k_1 t + \ln q_e \quad (12)$$

pseudo second order (PSO) model: $$\frac{t}{q_t} = \frac{1}{q_e} t + \frac{1}{k_2 q_e^2} \quad (13)$$

intra particle diffusion (IPD) model: $$q_t = k_i \sqrt{t} + C \quad (14)$$

where q_e and q_t are the concentrations of PHB at equilibrium and after time t, and k_0, k_1, k_2 and k_i are the equilibrium rate constants. According to the regression coefficient (R^2 = 0.9952), it can be concluded that the loading process of the PHB drug on the Fe_3O_4/NH_2-SBA-16 nanocomposite corresponds to the PFO model.

Table 7. Calculated Parameters of Adsorption Isotherms of the PHB Drug onto Fe_3O_4/NH_2-SBA-16

Temp. (K)	$\ln K_c$	ΔH° (kJ mol^{-1})	ΔS° (kJ mol$^{-1}K^{-1}$)	ΔG° (kJ mol^{-1})	R^2
303	3.42			-8.67	
313	2.96			-8.22	
323	2.87	-22.07	-0.04	-7.78	0.9944
333	2.64			-7.34	
343	2.36			-6.36	

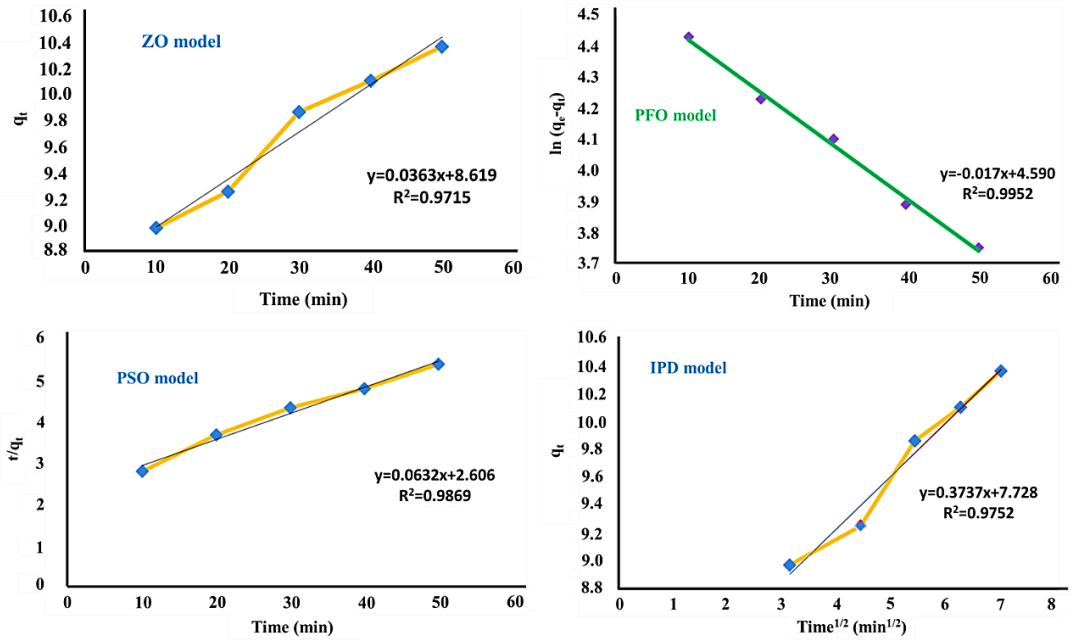

Fig. 14. Kinetic models for the absorption of PHB onto Fe_3O_4/NH_2-SBA-16.

Table 8. Kinetic Parameters for the PHB Loading onto Fe_3O_4/NH_2-SBA-16

Zero-order model (ZO)			Pseudo-first-order model (PFO)		
k_0 (M min^{-1})	q_e (mg g^{-1})	R^2	k_1 (min^{-1})	q_e (mg g^{-1})	R^2
0.0363	8.62	0.9715	0.0170	1.52	0.9952
Pseudo-second-order model (PSO)			Intra-particle diffusion (IPD)		
k_2 (M min^{-1})	q_e (mg g^{-1})	R^2	k_i (min^{-1})	q_e (mg g^{-1})	R^2
0.0017	15.82	0.9869	0.3737	7.73	0.9752

Drug Release Tests

In this research, three aqueous, acidic, and alkaline environments were used as external solutions (simulated body environment) for drug release. The aqueous environment was distilled water with pH = 6.8, and the acidic and alkaline environments were buffer solutions with pH = 4.6 and 7.8, respectively. Drug release was performed at 1, 2, 3, 4, 12, 24, 48, and 72 h (Fig. 15). In 2011, Zeng *et al.* presented a theoretical kinetic model to explain the drug release from silica nanoparticles [51]. This model suggests a two-step kinetics of the drug from the nanocomposite. In this model, it is assumed that the drug release has a fast release in the initial times and then a slow and stable release related to the release of drug molecules that are placed inside the pores of mesoporous silica nanoparticles.

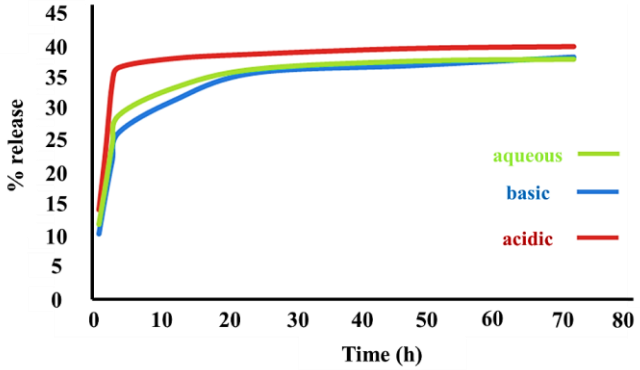

Fig. 15. *In vitro* release of PHB by Fe_3O_4/NH_2-SBA-16 mesoporous.

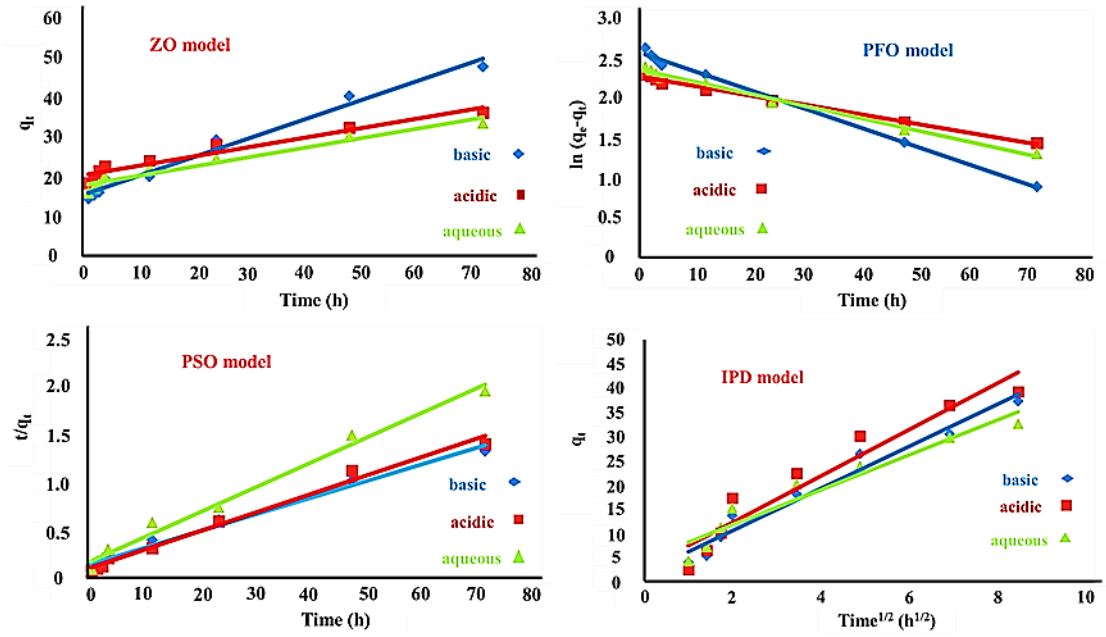

Fig. 16. Kinetic models for the release of the PHB drug.

Table 9. Kinetic Parameters for the Release of the PHB Drug

Zero-order model (ZO)				Pseudo-first-order model (PFO)			
Condition	k_0 (M min^{-1})	q_e (mg g^{-1})	R^2	Condition	k_1 (min^{-1})	q_e (mg g^{-1})	R^2
Aqua	0.4768	15.518	0.9777	Aqua	0.0236	0.947	0.9945
Acidic	0.2369	20.435	0.9473	Acidic	0.0118	0.822	0.9931
Basic	0.2374	17.799	0.9504	Basic	0.0153	0.860	0.9920
Pseudo-second-order model (PSO)				Intra-particle diffusion (IPD)			
Condition	k_2 (M^{-1} min^{-1})	q_e (mg g^{-1})	R^2	Condition	k_i (min^{-1})$^{1/2}$	q_e (mg g^{-1})	R^2
Aqua	0.0027	54.470	0.9849	Aqua	4.342	1.812	0.9639
Acidic	0.0044	51.540	0.9872	Acidic	4.798	2.612	0.9254
Basic	0.0045	38.460	0.9885	Basic	3.594	4.584	0.9319

In addition, the above models were used for drug release kinetics. The results in Fig. 16 and Table 9 show that the drug release also follows the first-order kinetics.

CONCLUSIONS

In this study, the Fe_3O_4/NH_2-SBA-16 mesostructure was synthesized as a nanocarrier for loading and release of the phenobarbital drug. To identify and characterize the properties of the SBA-16/NH_2 and Fe_3O_4/NH_2-SBA-16 nanostructures, several identification methods, such as X-ray diffraction analysis, Fourier transform infrared spectroscopy, nitrogen adsorption-adsorption isotherm, elemental analysis, scanning electron microscopy and transmission electron microscopy images, were used. The effects of variables including pH, drug concentration, nanocomposite dose, temperature, and contact time on absorption efficiency were studied by the response surface methodology and design of experiments software. Drug release in three different environments at 37 °C, including aqueous medium with pH = 7.0, acidic with pH = 4.6, and basic with pH = 7.8, at times of 1, 2, 3, 4, 12, 24, 48, and 72 h was studied. The data

obtained from isotherm determination studies and drug loading kinetics showed that the drug loading process follows the Langmuir isotherm with $R^2 = 0.9989$ and the quasi-first-order kinetics model with $R^2 = 0.9952$. The thermodynamic study also showed that the adsorption of the drug on the Fe_3O_4/NH_2-SBA-16 nanosilicate is an exothermic and spontaneous process at low temperatures.

ACKNOWLEDGEMENTS

This research is derived from a research project titled (Synthesis and application of Fe_3O_4/SBA-16-NH_2 nanoparticles as a phenobarbital drug delivery system) which was carried out with the financial support of Ayatollah Boroujerdi University and with tracking code IR.1-04-1401000755.

REFRENCES

[1] Gang Wang, A. N. O.; Blair, E. A.; Denton, K.; Tao, Z.; Asefa, T., Functionalized mesoporous materials for adsorption and release of different drug molecules: A comparative study. *J. Solid State Chem*. **2009**, *182*, 1649-1660, DOI: 10.1016/j.jssc.2009.03.034.

[2] Nejad, M. A.; Umst, P.; Urbassek, H. M., Boron nitride nanotubes as containers for targeted drug delivery of doxorubicin. *Journal of Molecular Modeling*. **2020**, *26*, 54-63, DOI: 10.1007/s00894-020-4305-z.

[3] Shi, Z. G.; Guo, Q. Z.; Liu, Y. T.; Xiao, Y. X.; Xu, L., Drug delivery devices based on macroporous silica spheres. *Mater. Chem. Phys*. **2011**, *126*, 826-831, https://doi.org/10.1016/j.matchemphys.2010.12.035.

[4] Li, Z.; Su, K.; Cheng, B.; Deng, Y., Organically modified MCM-type material preparation and its usage in controlled amoxicillin delivery. *J. Colloid Interface Sci*. **2010**, *342*, 607-613, DOI: 10.1016/j.jcis.2009.10.073.

[5] Yang, P.; Quan, Z.; Li, C.; Lian, H.; Huang, S.; Lin, J.; Fabrication, characterization of spherical $CaWO_4$: Ln@ MCM-41 (Ln = Eu^{3+}, Dy^{3+}, Sm^{3+}, r^{3+}) composites and their applications as drug releas systems, *Microporous Mesoporous Mater*. **2008**, *116*, 524-531. DOI: 10.1016/ j.micromeso.2008.05.016.

[6] Hwang, D. H.; Lee, D.; Lee, H.; Choe, D.; Lee, S. H.; Lee, K., Surface functionalization of SBA-15 particles for iburofen delivery. *Korean J. Chem. Eng*. **2010**, *27*, 1087-1092, DOI: 10.1007/s11814-010-0225-4.

[7] Uribe Madrid S. I.; Pal, U.; Kang, Y. S.; Kim, J.; Kwon, H.; Kim, J.; Fabrication of Fe_3O_4@mSiO_2 Core-Shell Composite Nanoparticles for Drug Delivery Applications. *Nanoscale Res. Lett.* **2015**, *10*, 217-225, DOI: 10.1186/s11671-015-0920-5.

[8] Seljak, K. B.; Kocbek, P.; Gašperlin, M.; Mesoporous silica nanoparticles as delivery carriers: An overview of drug, loading techniques. *J. Drug Delivery Sci. Technol*. **2020**, **59**, 101906, DOI: 10.1016/j.jddst.2020.01906.

[9] Hossen, S.; Hossain, M. K.; Basher, M. K.; Mia, M. N. H.; Rahman, M. T.; Uddin, M. J.; Smart nanocarrier-based drug delivery systems for cancer therapy and toxicity studies: A review. *J. Adv. Res*. **2019**, *15*, 1-18, https://doi.org/10.1016/j.jare.2018.06.005.

[10] Fekri, M. H.; Soleymani, S.; Razavi Mehr, M.; Akbari-adergani, B., Synthesis and characterization of mesoporous ZnO/SBA-16 nanocomposite: its efficiency as drug delivery system. *J. Non-Cryst. Solids*. **2022**, *591*, 121512, DOI: 10.1016/j.jnoncrysol.2022.121512.

[11] Wu, S. H.; Mou, C. Y., Lin, H. P., Synthesis of mesoporous silica nanoparticles. *Chem. Soc. Rev*. 2013, *42*, 3862-3875, https://doi.org/10.1039/C3CS35405A.

[12] Ijaz, A.; Yagci, M. B.; Ow-Yang; C. W.; Demirel, A. L.; Miko, A., Formation of mesoporous silica particles with hierarchical morphology. *Microporous Mesoporous Mater*. **2020**, *303*, 110240, DOI: 10.1016/ j.micromeso.2020.110240.

[13] Rivera-Muñoz, E. M.; Huirache-Acuña, R., Sol gel-derived SBA-16 mesoporous material. *Int. J. Mol. Sci.* **2010**, *11*, 3069-3086, DOI: 10.3390/ijms11093069.

[14] Wang, L.; Fan, J.; Tian, B.; Yang, H.; Yu, C.; Tu, B.; Zhao, D., Synthesis and characterization of small pore thick-walled SBA-16 templated by oligomeric surfactant with ultra-long hydrophilic chains. *Microporous Mesoporous Mater*. **2004**, *67*, 135-141, https://doi.org/10.1016/j.micromeso.2003.10.015.

[15] Soares, D. C. F.; Soares, L. M.; Goes, A. M.; Melo, E. M.; Barros, A. L. B.; Santos Bicalho, S.; Leao, N. M.; Tebaldi, M. L., Mesoporous SBA-16 silica nanoparticles as a potential vaccine adjuvant against Paracoccidioides brasiliensis. *Microporous and Mesoporous Materials*.

2020, *291*, 109676, https://doi.org/10.1016/j.micromeso.2019.109676.

[16] Costa, J. A. S.; de Jesus, R. A.; Santos, D. O.; Neris, J. B.; Figueiredo, R. T.; Paranhos, C. M., Synthesis, functionalization, and environmental application of silica-based mesoporous materials of the M41S and SBA-n families: A review. *Journal of Environmental Chemical Engineering*. **2021**, *9*, 105259, DOI: 10.1016/j.jece.2021.105259.

[17] Liu, M.; Ye, Y.; Ye, J.; Gao, T.; Wang, D.; Chen, G.; Song, Z., Recent advances of magnetite (Fe_3O_4)-based magnetic materials in catalytic applications. *Magnetochemistry*. **2023**, *9*, 110, https://doi.org/10.3390/magnetochemistry9040110.

[18] Chomoucka, J.; Drbohlavova, J.; Huska, D.; Adam, V.; Kizek, R.; Hubalek, J., Magnetic nanoparticles and targeted drug delivering. *Pharmacological Research*. **2010**, *62*, 144-149, https://doi.org/10.1016/j.phrs.2010.01.014.

[19] Barros, A. L. B.; Ferraz, K. S. O.; Dantas, T. C. S.; Andrade, G. F.; Cardoso, V. N.; Sousa, E. M. B., Synthesis, characterization, and biodistribution studies of (99m) Tc-labeled SBA-16 mesoporous silica nanoparticles. *Mater. Sci. Eng. C Mater. Biol. Appl*. **2015**, *1*, 181, DOI: 10.1016/j.msec.2015.06.030.

[20] Hudson, S. P.; Padera, R. F.; Langer, R.; Kohane, D. S., The biocompatibility of mesoporous silicates. *Biomaterials*. **2008**, *29*, 4045, DOI: 10.1016/j.biomaterials.2008.07.007.

[21] Ai, L.; Huang, H.; Chen, Z.; Wei, X.; Jiang, J., Activated carbon/$CoFe_3O_4$ composites: Facile synthesis, magnetic performance and their potential application for the removal of malachite green from water. *Chem. Eng. J*. **2010**, *156*, 243-249, https://doi.org/10.1016/j.cej.2009.08.028.

[22] Scioli-Montoto, S.; Sbaraglini, M. L.; Cisneros, J. S.; Chain, C. Y.; Ferretti, V.; León, I. E.; Ruiz, M. E., Novel phenobarbital-loaded nanostructured lipid carriers for epilepsy treatment: from QbD to *in vivo* evaluation. *Frontiers in Chemistry*. **2022**, *10*, 908386, DOI: 10.3389/fchem.2022.908386.

[23] Hemmat, A.; Ghassami, E.; Minaiyan, M.; Varshosaz, J., Magnetophoretic intranasal drug-loaded magnetic nano-aggregates as a platform for drug delivery in status epilepticus. *Pharmaceutical nanotechnology*. **2023**, *11*, 155, DOI: 10.2174/2211738511666230106154557.

[24] Mansour Lakouraj, M.; Norouzian, R. S.; Balo, S., Preparation and Cationic Dye Adsorption of Novel Fe_3O_4 Supermagnetic/Thiacalix [4] arene Tetrasulfonate Self-Doped/Polyaniline Nanocomposite: Kinetics, Isotherms, and Thermodynamic Study. *J. Chem. Eng. Data.* **2015**, *60*, 2262, DOI: 10.1021/acs.jced.5b00080.

[25] Sengupta, A.; Rao, R.; Bahadur, D., Zn^{2+}–Silica Modified Cobalt Ferrite Magnetic Nanostructured Composite for Efficient Adsorption of Cationic Pollutants from Water. *ACS Sustainable Chem. Eng*. 2017, **5**, 1280, https://doi.org/10.1021/acssuschemeng.6b01186.

[26] Girginova, P. L.; Daniel-da-Silva, A. L.; Lopes, C. B.; Figueira, P.; Otero, M.; Amaral, V. S.; Pereira, E.; Trindade, T. J., Silica Coated Magnetite Particles for Magnetic Removal of Hg^{2+} from Water. *Colloid Interface Sci*. 2010, **345**, 234-240, DOI: 10.1016/j.jcis.2010.01.087.

[27] Fekri, M. H.; Tousi, F.; Heydari, R.; Razavi Mehr, M.; Rashidipour, M., Synthesis of Magnetic Novel Hybrid Nanocomposite (Fe_3O_4@SiO_2/Activated carbon (by a Green method and Evaluation of Its Antibacterial Potential. *Iran. J. Chem. Chem. Eng*. **2022**, *41*, 767-776, DOI: 10.30492/ijcce.2021.128507.4164.

[28] Soleymani, S.; Razavi Mehr, M.; Fekri, M. H.; Saki, F.; Modification of SBA-16 surface by -NH_2 group and its application as adsorbent. *Chem. Pap*. **2023**, *77*, 5129-514, DOI: 10.1007/s11696-023-02849-6.

[29] Bakatula, E. N.; Richard, D.; Neculita, C. M.; Zagury, G. J., Determination of point of zero charge of natural organic materials. *Environ. Sci. Pollut. Res. Int*. **2018**, *25*, 7823-7833, doi:10.1007/s11356-017-1115-7.

[30] Fekri, M. H.; Shahverdi, V.; Chegeni, M.; Razavi Mehr, M.; Abbastabar Ahangar, H.; Saffar, A., Simultaneous photocatalytic degradation of cefixime and cefuroxime antibiotics using g-C_3N_4/$NaBiO_3$ nanocomposite and optimization of effective parameters by response surface methodology. *Reaction Kinetics, Mechanisms and Catalysis*. **2022**, *135*, 1059-1075, DOI: 10.1007/s11144-022-02192-z.

[31] Gupta, R.; Layek, S.; Pathak, D. D., Synthesis and characterization of guanine-functionalized mesoporous

silica [SBA-16-G]: a metal-free and recyclable heterogeneous solid base catalyst for synthesis of pyran-annulated heterocyclic compounds. *Res. Chem. Intermed*. **2019**, *45*, 1619-1637, DOI: 10.1007/s11164-018-3693-5.

[32] Feliczak-Guzik, A.; Jadach, B.; Piotrowska, H.; Murias, M.; Lulek, J.; Nowak, I., Synthesis and characterization of SBA-16 type mesoporous materials containing amine groups. *Microporous Mesoporous Mater*. **2016**, *220*, 231-238, https://doi.org/10.1016/j.micromeso.2015.09.006.

[33] Sayyadi, K.; Mohammadi, P.; Abaszadeh, M.; Sheibani, H., Au Nanoparticles Immobilized in Fe_3O_4/SBA-16 Functionalized Melamine-α-Chloroacetic Acid as a Recoverable Nanocatalyst for Reduction of Dye Pollutants in Water. *Chwmistry Select*. **2019**, *4*, 7609-7615, DOI: 10.1002/slct.201901421.

[34] Tang, S.; Zhao, M.; Yuan, D.; Li, X.; Wang, Z.; Zhang, X.; Jiao, T.; Ke, J., Fe_3O_4 nanoparticles three-dimensional electro-peroxydisulfate for improving tetracycline degradation. *Chemosphere*. **2021**, *268*, 129315, DOI: 10.1016/j.chemosphere.2020.129315.

[35] Bhuyan, D. M.; Saikia, M.; Saikia, L., Magnetically recoverable Fe_3O_4@SBA-15: An improvedcatalyst for three component coupling reaction of aldehyde, amine and alkyne. *Catal. Commun*. **2015**, *58*, 158-163, https://doi.org/10.1016/j.catcom.2014.09.011.

[36] Bhuyan, D.; Saikia, M.; Saikia, L., ZnO nanoparticles embedded in SBA-15 as an efficient heterogeneous catalyst for the synthesis of dihydropyrimidinones via Biginelli condensation reaction. *Microporous Mesoporous Mater*. **2018**, *256*, 39-48, https://doi.org/10.1016/j.micromeso.2017.06.052.

[37] Zhao, D.; Huo, Q.; Feng, J.; Chmelka, B. F.; Stucky, G. D., Nonionic triblock and diblock copolymer and oligomeric surfactant synthesis of highly orered, hydrothermally stable, mesoporous silica structure. *J. Am. Chem. Soc*. **1998**, *120*, 6024-636, DOI: 10.1021/JA974025I.

[38] Wen, H.; Zhou, X.; Shen, Z.; Peng, Z.; Chen, H.; Hao, L.; Zhou, H., Synthesis of ZnO nanoparticles supported on mesoporous SBA-15 with coordination effect –assist for anti-bacterial assessment. *Colloids Surf. B.* **2019**, *181*, 285-294, DOI: 10.1016/j.colsurfb.2019.05.055.

[39] Wang, X.; Mei, J.; Zhao, Z.; Chen, Z.; Zheng, P.; Fu, J.; Li, H.; Fan, J.; Duan, A.; Xu, C., Controllable synthesis of spherical Al-SBA-16 mesoporous materials with different crystal sizes and its high isomerization performance for hydrodesulfurization of Dibenzothiophene and 4,6-Dimethyldibenzothiophene. *Ind. Eng. Chem. Res.* **2018**, *57*, 2498-2507, https://doi.org/10.1021/acs.iecr.8b00109.

[40] Fekri, M. H.; Isanejad Mohamareh, S.; Hosseini, M.; Razavi Mehr, M., Green synthesis of activated carbon/Fe_3O_4 nanocomposite from flaxseed, its application as adsorbent and antibacterial. *Chem. Pap*. **2022**, *76*, 6767, doi: 10.1007/s11696-022-02278-x.

[41] Calignano, F.; Manfredi, D.; Ambrosio, E. P.; Iuliano, L.; Fino, P., Influence of process parameters on surface roughness of aluminum parts produced by DMLS. *Int. J. Adv. Manuf. Technol*. **2013**, *67*, 2743-2751, https://doi.org/10.1007/s00170-012-4688-9.

[42] Albayati, T. M.; Salih, I. K.; Alazzawi, H. F., Synthesis and characterization of a modified surface of SBA-15 mesoporous silica for a chloramphenicol drug delivery system. *Heliyon*. **2019**, *5*, e02539, https://doi.org/10.1016/j.heliyon.2019.e02539.

[43] Marahel, F.; Mombeeni, G. B.; Basari, N.; Niknam, L.; Ghazali, A. A., Applying Neural Network Model for Adsorption Methyl Paraben (MP) Dye Using Ricinus Communis-capeed Fe_3O_4 NPs Synthesized from Aqueous Solution. *J. Chem. Chem. Eng.* **2022**, *41*, 2358-2377, DOI: 1021-9986/2022/7/2358-2377.

[44] Aregawi, B. H.; Mengistie, A. A.; Removal of Ni(II) from aqueous solution using leaf, bark and seed of Moringa stenopetala adsorbents. *Bull. Chem. Soc. Ethiop*. **2013**, *27*, 35-47, DOI: 10.4314/bcse.v27i1.4.

[45] Ansari, R.; Banimahd Keivani, M.; Fallah Delavar, A., Application of polyaniline nanolayer composite as an efficient adsorbent for removal of tartrazine dye from aqueous solutions. *J. Polymer Research*. **2011**, *18*, 1931-1939, DOI: 10.1007/s10965-011-9600-z.

[46] Ansari, R.; Banimahd Keivani, M.; Fallah Delavar, A., Application of polypyrrole coated onto wood sawdust forremoval of carmoisine dye from aqueous solutions, *Journal of Applied Polymer Science*. **2011**, *122*, 804-812, DOI: 10.1002/app.34051.

[47] Shikuku, V. O.; Zanella, R.; Kowenje, C. O.; Donato, F. F.; Bandeira, N. M. G.; Prestes, O. D., Single and binary adsorption of sulfonamide antibiotics onto iron-modified clay: linear and nonlinear isotherms, kinetics, thermodynamics, and mechanistic studies. *Applied Water Science.* **2018**, *8*, 175-187, https://doi.org/10.1007/s13201-018-0825-4.

[48] Fekri, M. H.; Razavi Mehr, M.; Soleymani, S.; Saki, F., Fabrication and characterization of Ag/ZnO/SBA-16 Nano composite: its applications as drug delivery systems. *Phys. Chem. Res.* **2024**, *12*, 1111-1131, doi: 10.22036/pcr.2024.466280.2548.

[49] Razavi Mehr, M.; Fekri, M. H.; Omidali, F.; Eftekhari, N.; Akbari-adergani, B., Removal of Chromium(VI) from Wastewater by Palm Kernel Shell-based a Green Method. *Journal of Chemical Health Risks*. **2019**, *9*, 75-86, DOI: 10.22034/jchr.2019.584177.1012.

[50] PourShaban, M.; Moniri, E.; Safaeijavan, R.; Panahi Homayon, A., Kinetics, Isotherm and Adsorption Mechanism Studies of Letrozole Loaded Modified and Biosynthesized Silver Nanoparticles as a Drug Delivery System: Comparison of Nonlinear and Linear Analysis. *Korean Chem. Eng. Res.* **2021**, *59*, 493-502, https://doi.org/10.9713/kcer.2021.59.4.493.